Three-Dimensional Quantitative Structure−Activity Relationship of Nucleosides Acting at the A_3 Adenosine Receptor: Analysis of Binding and Relative Efficacy

Soo-Kyung Kim† and Kenneth A. Jacobson*

Molecular Recognition Section, Laboratory of Bioorganic Chemistry, National Institute of Diabetes and Digestive and Kidney Diseases (NIDDK), National Institutes of Health (NIH), Bethesda, Maryland 20892

Received November 8, 2006

The binding affinity and relative maximal efficacy of human A_3 adenosine receptor (AR) agonists were each subjected to ligand-based three-dimensional quantitative structure−activity relationship analysis. Comparative molecular field analysis (CoMFA) and comparative molecular similarity indices analysis (CoMSIA) used as training sets a series of 91 structurally diverse adenosine analogues with modifications at the N^6 and C2 positions of the adenine ring and at the 3′, 4′, and 5′ positions of the ribose moiety. The CoMFA and CoMSIA models yielded significant cross-validated q^2 values of 0.53 ($r^2 = 0.92$) and 0.59 ($r^2 = 0.92$), respectively, and were further validated by an external test set (25 adenosine derivatives), resulting in the best predictive r^2 values of 0.84 and 0.70 in each model. Both the CoMFA and the CoMSIA maps for steric or hydrophobic, electrostatic, and hydrogen-bonding interactions well reflected the nature of the putative binding site previously obtained by molecular docking. A conformationally restricted bulky group at the N^6 or C2 position of the adenine ring and a hydrophilic and/or H-bonding group at the 5′ position were predicted to increase A_3AR binding affinity. A small hydrophobic group at N^6 promotes receptor activation. A hydrophilic and hydrogen-bonding moiety at the 5′ position appears to contribute to the receptor activation process, associated with the conformational change of transmembrane domains 5, 6, and 7. The 3D-CoMFA/CoMSIA model correlates well with previous receptor-docking results, current data of A_3AR agonists, and the successful conversion of the A_3AR agonist into antagonists by substitution (at N^6) or conformational constraint (at 5′-*N*-methyluronamide).

INTRODUCTION

Adenosine receptors (ARs), members of rhodopsin family A of G-protein-coupled receptors, have four different subtypes: A_1, A_{2A}, A_{2B}, and A_3.[1] A wide range of potential therapeutic applications for subtype-selective AR agonists are described in numerous papers and patents, indicating that ARs are a good target in drug development.[2] At present, only endogenous adenosine is used as a commercial pharmaceutical, for the treatment of arrhythmias and paroxysmal supraventricular tachycardia and in cardiac imaging.[3,4] However, numerous adenosine derivatives have been reported over the past 20 years as selective AR agonists. Several selective agonists are undergoing clinical trials for the treatment of cardiovascular diseases (at A_1 and A_{2A} receptors), pain (at A_1 receptors), and wound healing and diabetic foot ulcers (at A_{2A} receptors).[2] Our current research targets include the design of A_3AR agonists, which prevent ischemic damage in the brain and heart and exhibit anti-inflammatory, anticancer, and myeloprotective effects. The compound N^6-(3-iodobenzyl)-5′-*N*-methylcarboxamidoadenosine (IB-MECA), which we introduced as a selective A_3AR agonist, is undergoing phase II clinical studies for the treatment of metastatic colorectal tumors and rheumatoid arthritis.[5,6]

Although ARs are becoming important targets in drug development, several major problems complicate the development of AR agonists: (1) The ubiquitous expression of ARs in the body would result in diverse side effects. (2) The low density of a given receptor subtype in a targeted tissue may reduce its desired effect in the treatment of certain diseases. An example is the A_3AR, for which selective agonists have been described as promising cardio- and cerebroprotective agents. However, the low density of the A_3AR in the heart may be a problem.[2] (3) In many cases, nucleoside derivatives have lowered maximal efficacy (the ability of a bound ligand to induce the required conformational change of the receptor in order to activate an effector) at the A_3AR and, consequently, display the pharmacological characteristics of a partial agonist or antagonist. Thus, to develop selective A_3AR agonists, both the binding affinity at each subtype and the agonist efficacy should be studied. (4) Obtaining three-dimensional (3D) structural information about G-protein-coupled receptors is not yet feasible through the application of standard structure determination techniques—X-ray and nuclear magnetic resonance studies—because of the difficulties in receptor purification and their insolubility in environments lacking phospholipids. This is a major bottleneck for structure-based drug design. Therefore, in cases where the receptor structure is unknown, a ligand-based approach, based only on an extensive study of structure−activity relationships (SARs), could be informative.

The SAR of various adenosine substitutions suggests the possibility of specifically designing ligands to achieve a

* Corresponding author: Dr. K. A. Jacobson, Chief, Molecular Recognition Section, Bldg. 8A, Rm. B1A-19, NIH, NIDDK, LBC, Bethesda, Maryland 20892-0810. Tel.: 301-496-9024. Fax: 301-480-8422. E-mail: kajacobs@helix.nih.gov.

† Current address: Biomacromolecular Modeling Section, Beckman Institute (Mail Stop: 139-74), California Institute of Technology, 1200 E. California Blvd., Pasadena, CA 91125.

10.1021/ci600501z CCC: $37.00
Published on Web 03/06/2007

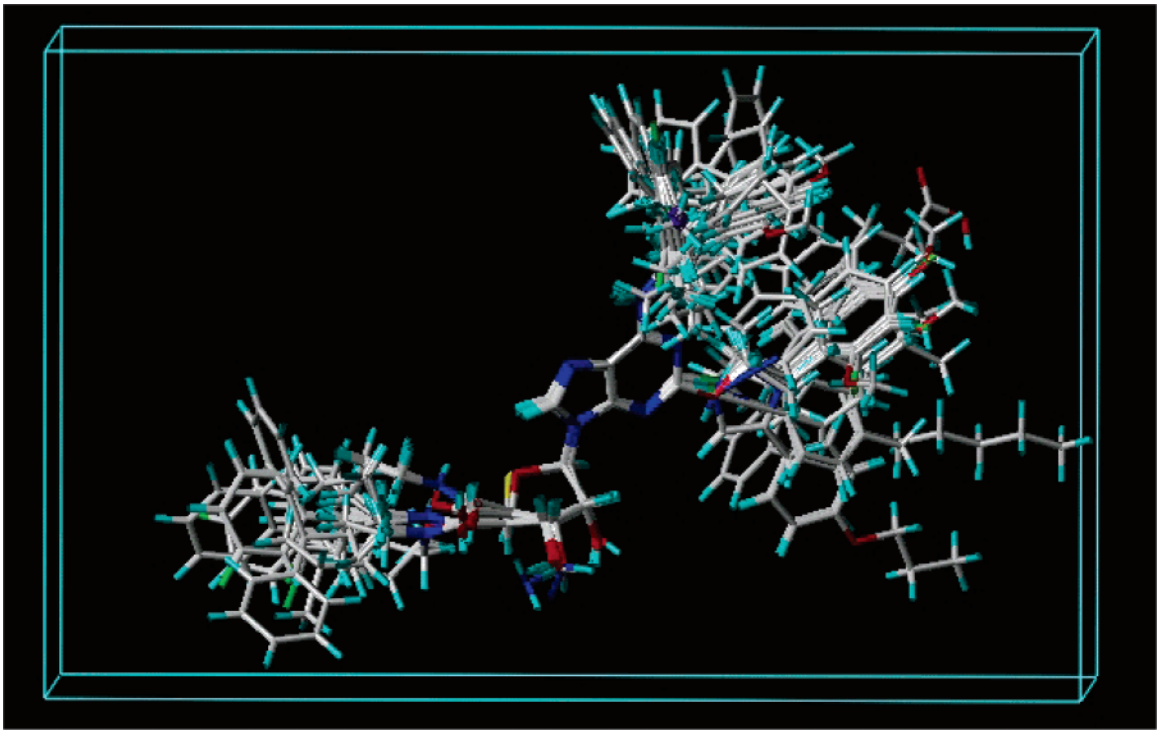

Figure 1. Alignment of all adenosine derivatives from the training set in a defined region ($X = -22$ to -2, $Y = -16$ to $+16$, $Z = -8$ to $+8$). Adenosine **1**, an endogenous agonist, was selected as the template for aligning the compounds in the training sets. All 91 molecules from the training set database (Figure I in the Supporting Information) were suitably aligned into a similar orientation in Cartesian space using the Align Database module. Specifically, all heteroatoms in adenosine except for the 4′-O atom were included, because 4′-thioadenosine derivatives are found in the database for the alignment.

desired pharmacological profile. The pharmacological parameters at the A_3AR considered in this study include affinity (as determined in competitive radioligand binding assays using membranes of cells expressing the receptor) and the relative maximal efficacy (in comparison to the ability of a known full agonist at a fixed high concentration to activate second messenger effects). The receptor subtype selectivity (affinity at the A_3AR in comparison with other AR subtypes) is available but not analyzed quantitatively in this study. The relative efficacy of adenosine derivatives at the A_3AR depends on distinct structural determinants. Recently, adenosine receptor agonists and antagonists have been the subject of modeling efforts.[7−12] Several of these efforts have successfully employed comparative molecular field analysis (CoMFA),[10,11] which develops a predictive 3D model on the basis of differences in steric/electrostatic fields and binding affinities. However, predictive models for adenosine A_3 agonists are presently unavailable. Therefore, in this study, we present the correlation of a diverse group of adenosine structural modifications with the binding affinity/maximal efficacy to predict new, highly potent, and selective agonists at the human (h) A_3AR with the quantitative 3D-SAR (3D-QSAR) techniques of CoMFA and comparative molecular similarity indices analysis (CoMSIA).[13] Statistically significant and highly predictive models offer utility in the rational design of potent and selective A_3AR agonists for therapeutic applications.

RESULTS AND DISCUSSION

Generation of Data Sets. Representative data from previously published studies[14−21] that used identical binding assay protocols were selected for current 3D-QSAR studies. The binding affinities of the synthesized adenosine derivatives were measured at the hA_3AR using the radiolabeled competitive binding agonist N^6-(4-amino-3-iodobenzyl)-adenosine-5′-*N*-methyluronamide, and their relative maximal efficacy in the activation of the A_3AR was determined in an assay of the inhibition forskolin-stimulated adenylyl cyclase. The functional data were expressed as a percent of the effect of the full agonist 5′-*N*-ethylcarboxamidoadenosine (**24**) at 10 μM. We used a data set containing 91 structurally diverse adenosine analogues (Figure I in the Supporting Information, compounds **1**−**91**), which were modified at the N^6 and the C2 positions of the adenine ring, and the 3′, the 4′, and the 5′ positions of the ribose group (except endogenous adenosine **1**) within various binding affinities (K_i) at the hA_3AR (Table I in the Supporting Information).

For the training set, structurally diverse C2-, N^6-, 3′-, and/or 5′-modified adenosine analogues were selected for the 3D-QSAR studies. A series of energetically favorable conformations optimized by the Merck molecular force field 94 (MMFF94)[32] were aligned in 3D-Cartesian space with an adenosine template (Figure 1).

3D-QSAR Modeling. As indicated in Table 1, diverse models with different energy fields (CoMFA, CoMFA-HB, and CoMSIA) and lattice spacing (1 or 2 Å) for the binding affinity of the A_3AR (CoMFA-1/2, CoMFA-HB1/2, and CoMSIA-1/2) and a single CoMSIA model for the relative efficacy at the A_3AR (CoMSIA-EFF) were generated. Each of these models displayed statistical significance ($r^2 > 0.8$) and internal predictive ability ($q^2 > 0.4$) for a total of 91 compounds. The CoMFA models with region focusing, CoMFA-RF1 (Table 1 and Figure 2A) and CoMFA-RF2, yielded excellent models, with $q^2 = 0.53$ and $r^2 = 0.92$ and

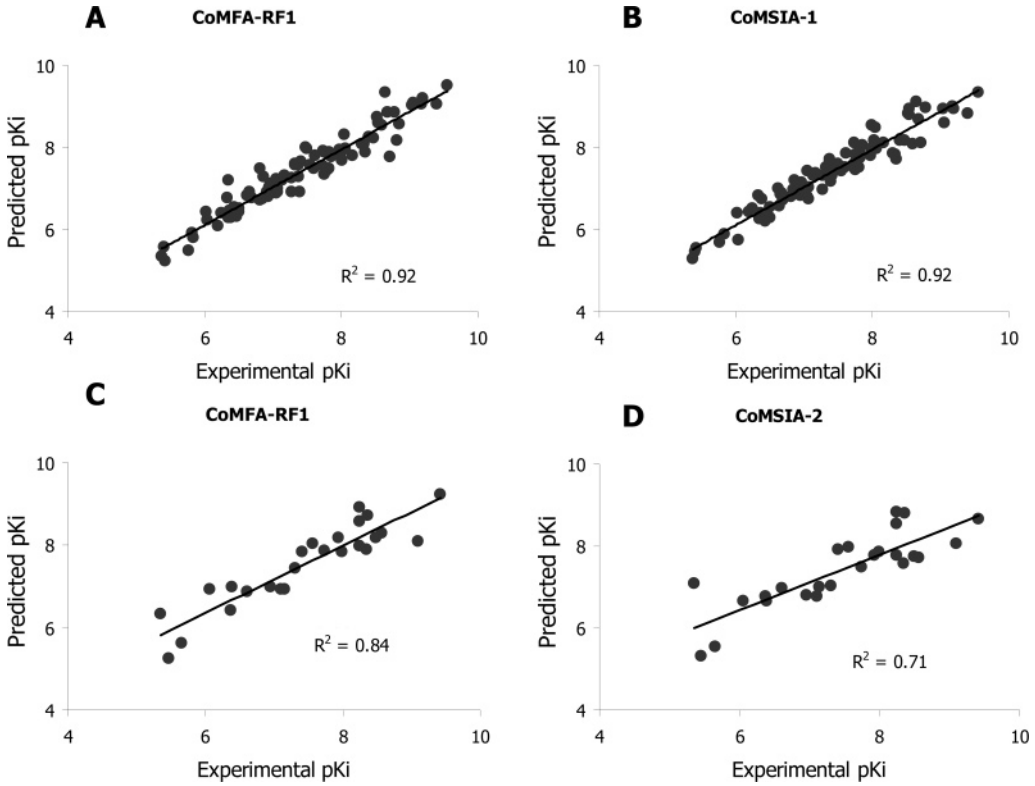

Figure 2. Fitted predictions versus experimental A_3AR binding affinities for the 91 compounds in the training sets and the 25 compounds in the test sets. (A) CoMFA-RF1 and (B) CoMSIA-2 in the training set and (C) CoMFA-RF1 and (D) COMSIA-2 in the test sets.

Table 1. The Partial Least Square (PLS) Results of the CoMFA and CoMSIA Analyses[a]

lattice spacing	PLS statistics	CoMFA	CoMFA-RF[b]	CoMFA-HB[b]	CoMSIA	CoMSIA-EFF[b]
2 Å	q^2	0.48	0.50	0.44	0.57 (4)	0.53 (4)
	r^2	0.90	0.83	0.83	0.91	0.91
	standard error of estimate	0.33	0.42	0.42	0.30	1.26
	F values	100.81	68.01	70.11	101.36	95.07
	PLS components	7	6	6	8	8
			Field Contribution (%)			
	steric	61.0	56.4	35.6	18.8	17.7
	electrostatic	39.0	43.6	19.2	26.0	27.6
	hydrophobic			25.7	31.3	31.0
	HB donor			19.5	16.4	16.1
	HB acceptor				7.5	7.6
1 Å	q^2	0.53	0.53	0.48	0.59 (5)	
	r^2	0.91	0.92	0.84	0.92	
	standard error of estimate	0.31	0.29	0.40	0.28	
	F values	121.92	117.41	90.27	115.58	
	PLS components	7	8	5	8	
			Field Contribution (%)			
	steric	57.0	49.4	31.1	18.3	
	electrostatic	43.0	50.6	19.7	27.8	
	hydrophobic			19.9	30.1	
	HB donor			29.3	16.3	
	HB acceptor				7.4	

[a] The numbers in parentheses represent the number of outliers in the residual plots from the cross-validation analyses. [b] RF, region focusing; HB, H-bonding; EFF, relative efficacy.

$q^2 = 0.50$ and $r^2 = 0.83$. Since the CoMSIA-1, CoMFA-RF2, CoMSIA-EFF models displayed poorer correlations, with $q^2 = 0.44$ and $r^2 = 0.79$, $q^2 = 0.43$ and $r^2 = 0.79$, and $q^2 = 0.37$ and $r^2 = 0.73$, respectively, the outliers in the residual plot from the cross-validation analyses were omitted for better predictability, with a sufficiently high q^2 (>0.5) and r^2 value (>0.9). The following compounds were detected as outliers from the CoMSIA models: **25**, **56**, **62**, **68**, and **73** for CoMSIA-1; **25**, **56**, **68**, and **73** for CoMSIA-2; and **25**, **50**, **66**, and **69** for CoMSIA-EFF. The most commonly detected outlier, 4′-thioadenosine **25**, exhibited an unexpected lowered binding affinity compared with the best compound, N^6-Me-2-Cl-4′-thio-5′-alkyluronamide adenosine **72** (hA_3 K_i = 0.28 nM) as well as 0% efficacy (antagonist). Five out of eight outliers were 4′-thioadenosine analogues, indicating the possibility of a subtle difference in the binding mode and

Table 2. Measured and Predicted Binding Affinities and Relative Efficacies of Adenosine Derivatives at Human A_3ARs in the Test Set[a]

		predicted binding affinities (pK_i)									
#	pK_i at hA_3R	CoMFA-2	CoMFA-1	CoMFA-RF2	CoMFA-RF1	CoMFA-HB2	CoMFA-HB1	CoMSIA-2	CoMSIA-1	eff. (%)	pred. eff. (%)
92	8.24	7.77	7.99	7.55	7.91	7.19	7.43	7.78	7.65	46.0	94.0
93	7.41	7.84	7.85	8.02	7.90	7.45	7.48	7.92	7.97	98.0	84.1
94	6.39	6.85	6.99	7.06	7.25	7.58	7.33	6.67	6.75	49.0	56.5
95	7.15	6.81	6.94	6.92	6.78	6.84	6.85	7.00	6.92	16.2	−10.9
96	7.11	6.88	6.94	6.71	6.83	7.04	6.86	6.77	6.76	44.5	23.9
97	6.95	6.96	6.98	6.61	6.91	7.09	6.98	6.80	6.80	73.4	55.7
98	6.06	6.87	6.92	6.68	6.88	7.08	7.05	6.67	6.66	66.5	107
99	6.60	6.89	6.88	6.79	6.91	6.94	7.04	6.96	6.91	19.3	81.2
100	6.37	6.38	6.41	6.84	6.92	6.76	6.74	6.78	6.73	9.80	0.88
101	8.35	7.72	7.91	8.24	7.94	7.59	7.91	7.56	7.54	0	7.50
102	7.93	7.92	8.19	8.06	7.64	7.66	7.78	7.78	7.71	3.40	6.59
103	7.99	7.50	7.85	7.81	7.50	7.29	7.73	7.85	7.79	11.4	29.5
104	8.56	8.44	8.30	8.14	8.11	7.35	7.55	7.71	7.69	29.0	80.6
105	8.25	8.50	8.57	8.68	8.56	7.83	8.50	8.53	8.80	86.0	58.4
106	5.65	5.69	5.63	6.15	5.48	5.31	5.71	5.55	5.54	0.00	2.46
107	9.10	8.13	8.09	8.07	7.90	7.74	8.22	8.06	8.22	96.0	55.4
108	7.74	7.89	7.86	7.99	7.61	7.29	8.09	7.48	7.79	63.0	62.5
109	7.31	7.50	7.45	7.47	7.40	7.02	7.85	7.02	7.28	62.0	47.3
110	8.49	8.21	8.17	8.18	7.94	7.35	8.12	7.75	7.84	32.0	59.0
111	5.46	5.55	5.24	5.05	4.72	4.43	4.86	5.31	5.36	3.10	−6.61
112	8.25	9.14	8.92	8.92	8.86	8.20	8.59	8.83	8.84	85.0	114
113	5.35	6.50	6.32	6.27	5.93	5.76	5.98	7.09	7.18	83.0	60.9
114	8.37	8.89	8.73	9.01	8.87	8.49	9.01	8.80	8.87	105	102
115	7.56	7.99	8.02	7.95	7.97	7.58	8.21	7.96	8.05	91.0	99.0
116	9.42	9.25	9.25	9.10	9.46	8.22	9.22	8.67	8.66	114	89.4

[a] Refer to Figure I (Supporting Information) for structures of the adenosine derivatives.

activation mechanisms of 4′-thioadenosine analogues in comparison to the oxo analogues. The corresponding CoMSIA models (CoMSIA-1, CoMSIA-2, and CoMSIA-EFF) yielded better values, with $q^2 = 0.59$ and $r^2 = 0.92$, $q^2 = 0.57$ and $r^2 = 0.91$, and $q^2 = 0.53$ and $r^2 = 0.91$, after removing some outliers. The strong correlation between observed and predicted pK_i values for the A_3AR is indicated in Table II in the Supporting Information and Figure 2B. In addition, the result of CoMSIA for A_3AR activation was attributed to the important contributions of hydrophobic and H-bonding interactions for A_3AR activation (Figure III in the Supporting Information and Table 1).

Validation of Models by External Test Sets. As a test set (Figure I, compounds **92**−**116**, and Table III in the Supporting Information), 25 structurally diverse C2-, N^6-, 3′-, and/or 5′-modified adenosine analogues were selected from previous studies such that there was a 4 log-unit difference between the highest (**116**, $pK_i = 9.42$) and the lowest (**113**, $pK_i = 5.35$) binding affinities and an even distribution within that range. The results are shown in Table 2 and Figure 2C and D. Each model generated highly predictive r^2 values: 0.84 in the CoMFA-1, 0.81 in the CoMFA-2, 0.80 in the CoMFA-RF2, 0.78 in the CoMFA-RF1, 0.76 in the CoMFA-HB1, 0.71 in the CoMSIA-2, 0.69 in the CoMSIA-1, and 0.63 in the CoMFA-HB2, while the CoMSIA-EFF model resulted in low correlations, with a 0.55 r^2 value. The excellent predictability across a broad range of structurally diverse A_3AR agonists suggests that these 3D-QSAR models are valuable tools for guiding the rational design of novel A_3AR agonists and for predicting both their binding affinities and their relative efficacies prior to synthesis and biological testing.

3D-QSAR Models for A_3AR Binding. This 3D-QSAR study provides a more detailed understanding of the binding domains of this AR, highlighting the key structural features required for receptor affinity and subtype selectivity. Similar contributions to the CoMFA-RF1 model were ascribed to steric (49.4%) and electrostatic (50.6%) interactions. The steric and electrostatic CoMFA color contour maps associated with differences in the A_3AR binding affinity demonstrate that the variations are dominated by structures at the N^6, 3′, and 5′ positions. In Figure 3A, a large green polyhedron favoring sterically bulky substituents at the site of N^6 substitution and a small green polyhedron at the C2 position were displayed, while a large yellow polyhedron was present around the 5′ position, correlating with known SAR data: **85** with 5′-ethyluronamide (hA_3AR $K_i = 0.89$ nM) versus **90** with 5′-phenylethyluronamide (hA_3AR $K_i = 433$ nM) compared to tolerable bulky residues at N^6 and C2. Yellow regions favoring less steric bulk were also present at the N^6 and C2 sites, indicating the importance in A_3AR recognition of the bound conformations of bulky substituents, when they are present at these positions. In the CoMFA electrostatic map (Figure 3B), regions favoring negative charge and positive charge were located around the 5′-carbonyl oxygen and the nitrogen atom of the 5′-NH group, respectively.

The CoMSIA hydrophobic map was consistent with the CoMFA steric map, illustrating a major hydrophobic region and a minor hydrophilic region at the N^6 and C2 positions, respectively. A hydrogen-bond (HB) donor was required at the H atom of the 5′-amide group consistent with its experimental result: **72** (5′-*N*-methyluronamide, hA_3 $K_i = 0.28$ nM) versus **73** (5′-*N*,*N*-dimethyluronamide, hA_3 $K_i = 1500$ nM). However, a HB acceptor is ideal at the 4′-O and the 5′-amide O atoms (Figure 3C and D).

3D-QSAR Models for A_3AR Activation. This 3D-QSAR study also displayed the essential structural features required for A_3AR activation.[23] The steric and electrostatic CoMFA

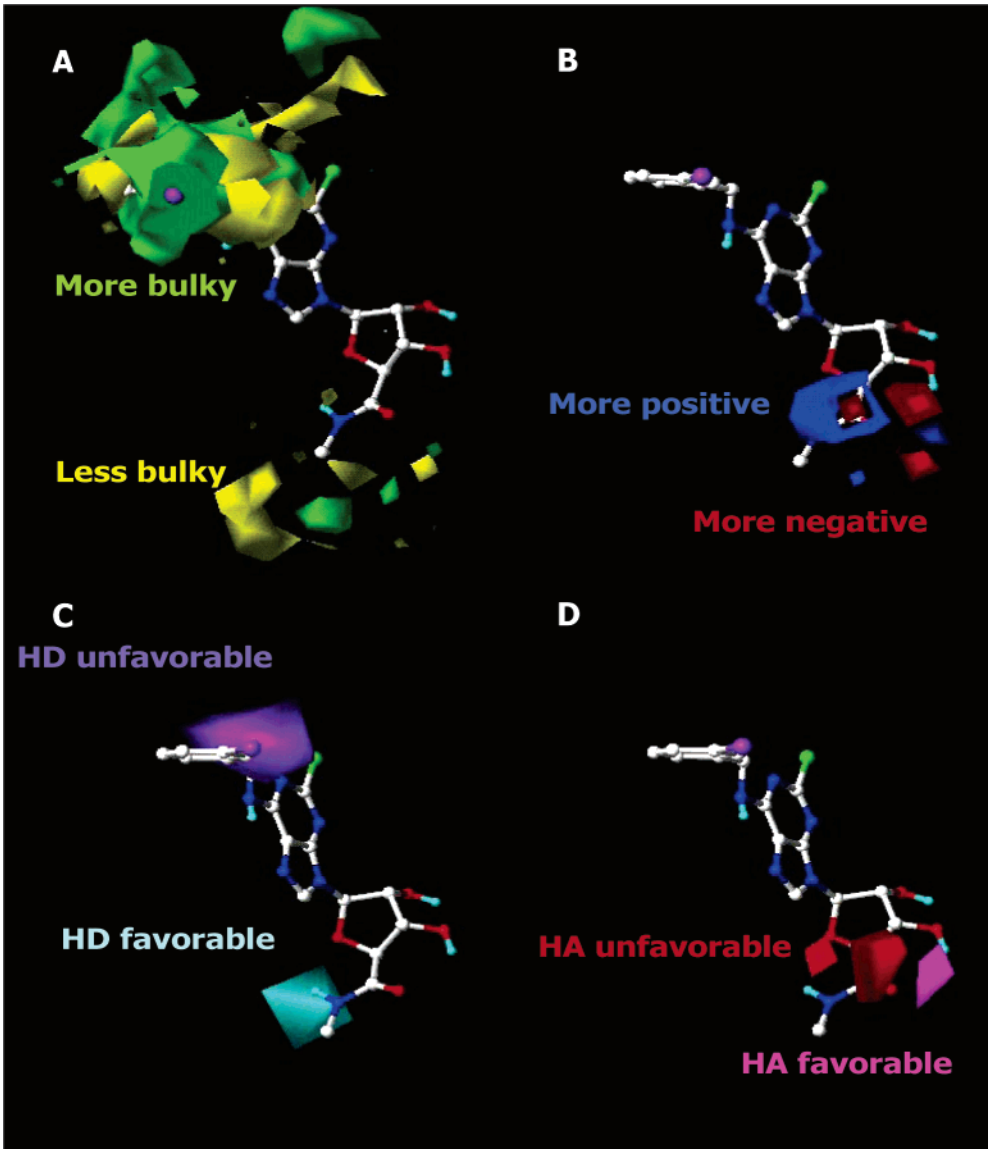

Figure 3. 3D representation of ligand properties favoring A_3AR binding affinity. The steric (A) and electrostatic (B) CoMFA maps of the CoMFA-RF1 model. The H-bonding donor (C) and acceptor (D) CoMSIA maps of the CoMSIA-2 model. Cl-IB-MECA **68** is shown as a representative ligand. The visualization of the CoMFA and CoMSIA maps has been performed with the StDev*Coefficient mapping option contoured by contribution. Favored and disfavored levels were fixed at 80% and 20%, respectively, for all fields. The steric contours are shown in green for regions tolerating groups of increased sterical bulk and yellow for regions favoring less bulky groups. The electrostatic maps are represented with blue contours indicating the regions where positive groups increased activity and red contours indicating regions where a negative charge increased activity. In the CoMSIA result, the H-bond field contours show H-bond acceptor (HA)-favored regions in magenta and disfavored regions in red and H-bond donor (HD)-favored regions in cyan and disfavored regions in purple. A hydrophobicity CoMSIA map of the CoMSIA-2 model is shown in Figure III in the Supporting Information.

color contour maps associated with differences in the A_3AR relative efficacy demonstrate that variations are dominated by structures at the N^6, C2, and 5′ positions. The hydrophobic and the H-bonding maps from the CoMSIA-EFF model are shown in Figure 4. A major region that favors less steric bulk was present at the site of N^6 substitution, and a minor such region was present the at the C2 position, while a large green polyhedron (steric bulk preferred) was also present around the C2 position. Green and yellow polyhedra of similar size appeared at the 5′ position (Figure 4A).

In the CoMSIA-EFF H-bonding map, a H-bonding (HB) donor was favored at the 5′-amide NH and the N^6 H atom (Figure 4B), while a HB acceptor similar to the CoMSIA HB acceptor map was favored at the 5′-CO oxygen atom. In the CoMSIA-EFF electrostatic map, regions requiring a negative charge and a positive charge, similar to the CoMFA and the CoMSIA models, were located around the 5′-carbonyl oxygen and the nitrogen atom of the 5′-NH group, respectively. The model is consistent with published results: **92** (N^6-3-I-benzyl, hA_3 efficacy = 46%) versus **68** (N^6-3-I-benzyl with 5′-*N*-methyluronamide, hA_3 efficacy = 100%) and **72** (5′-*N*-methyluronamide, hA_3 efficacy = 119%) versus **73** (5′-*N*,*N*-dimethyluronamide, hA_3 efficacy = 8.3%). Although the efficacy reducing factors of N^6-benzyl with 2-Cl and a methanocarba ring were present, the 5′-uronamide group always restored the efficacy. Finally, we could successfully convert an A_3AR agonist into a selective antagonist by the introduction of a spirolactam derivative at the 5′ position[24] or the substitution of a 5′-*N*,*N*-dimethyluronamide through removing the H-bonding donor ability at the 5′ position.[28] Thus, the CoMSIA-EFF model suggested that 5′-hydrophilic and/or 5′-H-bonding donor/acceptor groups

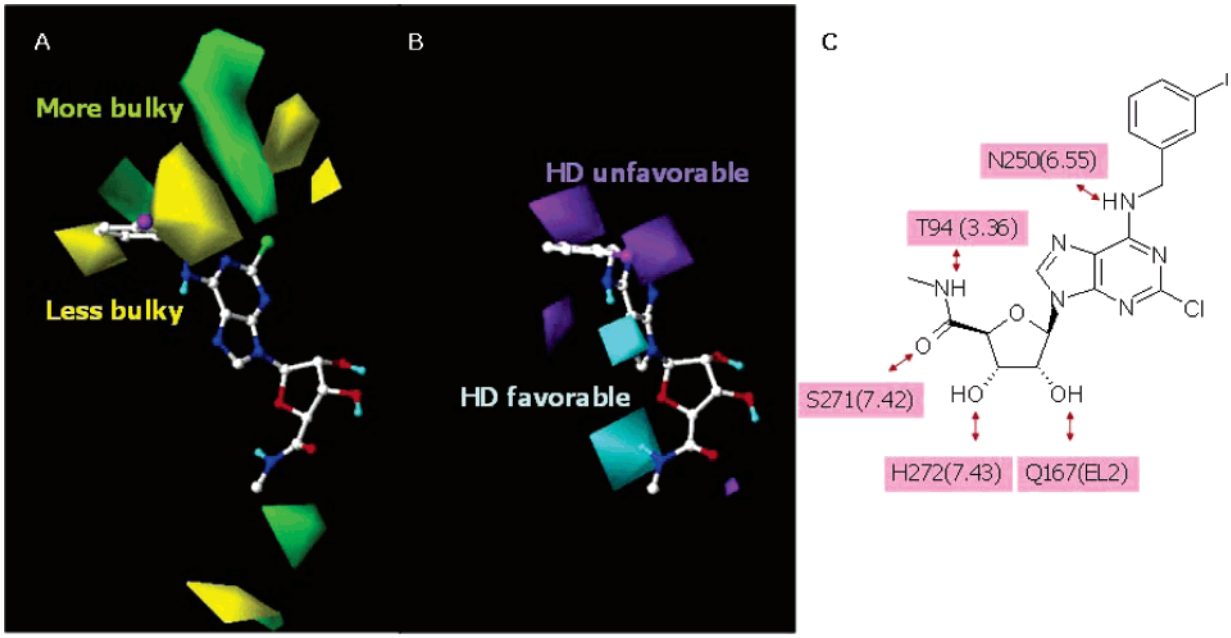

Figure 4. The CoMSIA maps of the CoMSIA-EFF model favoring relative efficacy in the activation of the A_3AR. Cl-IB-MECA **68** was used as a representative ligand for (A) the steric map, (B) the H-bond donor map, and (C) a schematic representation of putative receptor interactions. The visualization of the CoMSIA map has been performed using the StDev*Coefficient mapping option contoured by contribution. Favored and disfavored levels fixed at 80% and 20%, respectively, were used for all fields. In the CoMSIA result, the steric contours were shown in green for regions tolerating groups of increased steric bulk groups and yellow for regions favoring less bulky groups to increase the efficacy of the A_3AR. The H-bond field contours for the efficacy of the A_3AR show H-bond donor-favored regions in cyan and disfavored regions in purple.

and a N^6 small group appeared to be important for activation of the A_3AR.

Comparison of 3D-QSAR with Docking Models and Activation Mechanisms. To support the CoMFA/CoMSIA maps, the 3D contour maps were compared with the previously docked agonist−hA_3AR complex[24] with respect to amino acids surrounding the putative binding site. Mutagenesis results were consistent with molecular modeling that featured direct interaction of ligands with transmembrane domains (TMs) 3, 6, and 7 and with extracellular loop 2 (EL2).[25] A brief summary of the docking result for adenosine 5′-uronamides follows (Figure 4C and the Supporting Information).

The binding site of 2-chloro-N^6-(3-iodobenzyl)-5′-*N*-methylcarboxamidoadenosine (Cl-IB-MECA **68**) in the A_3AR was studied, illustrating the Connolly electrostatic potential surface of the protein (Figure II in the Supporting Information). When the 3D-QSAR maps were compared, the presence and location of sterically disfavored regions recognized by the CoMFA and CoMSIA models agreed well with the contour of the 3D receptor model. Compared with the large, hydrophobic N^6-binding region close to EL2, the binding site of the 5′ position appears to be of constricted space and is directed toward the inner TM region. The presence of mapped regions requiring less bulky groups indicates a specific active conformation at the N^6 and C2 positions, correlating well with the experimental results from the use of sterically constrained N^6-(2-phenylethyl)adenosine derivatives as hA_3AR-selective agonists.[14] In summary, each of the CoMFA electrostatic and CoMSIA H-bonding maps matched well with its surrounding amino acids in the putative agonist-binding site of the hA_3AR, and the 5′-uronamide group was an essential moiety for A_3AR binding.

The combination of docking studies and 3D-QSAR models was helpful in understanding the molecular mechanisms of receptor activation and ligand binding. (1) SAR studies showed that small N^6-alkyl groups increased binding affinity, while bulkier aliphatic rings lowered both efficacy and binding affinity at the hA_3AR. (2) The existence of regions requiring less bulky and more bulky groups that diverge from each other at the 5′ position suggested the optimized chain length for A_3AR activation. Compounds with long alkyl chains at the 5′ position—**78** (5′-(3,3-diphenylpropyl)uronamide), **81** (5′-(4-benzylpiperidine)carbonyl), and **90** (5′-(2-phenylethyl)uronamide)—displayed almost no efficacy, while corresponding compounds with short chains at the 5′ position (**72** and **79**) or with a 5′-*N*-methyl or *N*-ethyluronamide group (**85**) displayed 100% efficacy. (3) Both a region requiring a HB donor at the 5′-NH and a region requiring an acceptor at the 5′-CO group from the CoMSIA-EFF model were located at the side chains of T94 (3.36) and S271 (7.41) in the putative binding site. It was reported that alkylthio substituents at the 5′ position induced partial agonism at the A_3ARs.[27] The low efficacy of 5′-thioether derivatives is consistent with the need for H bonding in this region to activate the A_3AR. In a recent study, two selective A_3AR agonists, Cl-IB-MECA **68** and its 4′-thio analogue 2-chloro-N^6-(3-iodobenzyl)-5′-*N*-methylcarboxamido-4′-thioadenosine **116**, were successfully transformed into selective A_3AR antagonists by appending an additional *N*-methyl group on the 5′-uronamide position.[28] The 5′-(*N*,*N*-dimethyl)uronamido group especially tends to preserve affinity and selectivity in N^6-3-iodobenzyladenosine derivatives, while entirely abolishing activation of the hA_3AR. The additional experimental result supports the map that favors the H-bonding donor at the 5′-NH group in the CoMSIA-EFF model. Thus, the

CoMSIA-EFF maps were consistent with the activation results.

Two factors favored the binding of agonists and the resultant characteristic side-chain movements of TM6 and TM7: (1) additional H-bonding of the ribose 3′ and 5′ substituents with the hydrophilic amino acids $T^{3.36}$, $S^{7.42}$, and $H^{7.43}$ and (2) hydrophobic interaction of the terminal methyl group of the 5′-uronamide of Cl-IB-MECA **68** with the hydrophobic side chain of $F^{6.44}$. The map favoring a HB donor at the 5′-amide NH and the map favoring a HB acceptor at the 5′-CO atom from the present 3D-QSAR study correlated well with a previous modeling study of putative conformational changes of the receptor associated with activation.[23] That study postulated the involvement in receptor activation of specific HBs between the 5′ region of adenosine derivatives and the receptor.

The excellent correlation with previous receptor-docking results, the current SAR data of A_3AR agonists, and the successful cases of conversion of A_3AR agonists into antagonists suggest that these 3D-QSAR models are valuable computational tools for both the rational design of novel A_3AR agonists and the prediction of agonist properties prior to experimentation. However, further experiments are needed to validate a given model using reversed HB donating and accepting substituents and/or conformationally constrained bulky residues in the 5′ region. Nevertheless, our predictions help to delineate the ligand binding and activation mechanisms of hA_3AR.

CONCLUSIONS

The CoMFA and CoMSIA 3D-QSAR models were based on a training set consisting of 91 potent and structurally diverse A_3AR agonists and then validated by an external test set of 25 adenosine analogues. The CoMFA and CoMSIA analyses yielded significant cross-validated q^2 values of 0.53 ($r^2 = 0.92$) and 0.59 ($r^2 = 0.92$), respectively. The projection of the CoMFA/CoMSIA contour maps onto the putative agonist-binding site, which was validated by the experimental results, displayed good complementarity. The results of the CoMFA/CoMSIA study provided insight into the conformational and binding requirements for agonists at the A_3AR. A significant distinction between the models related to binding affinity and the relative efficacy of agonists was determined by whether H-bonding ability at the 5′ position was present or not. The previous docking result indicated that the introduction of a hydrophilic moiety such as ribose destabilizes the inactive ground state of the receptor and facilitates activation. In this study, we conclude that conformationally restricted bulky groups at the N^6 or C2 positions of the adenine ring and hydrophilic and/or H-bonding groups at the 5′ position increase A_3AR binding affinity. A small bulky group at N^6, a 5′-hydrophilic moiety, and/or a 5′ H-bonding moiety might be crucial for A_3AR activation. The 3D-CoMFA/CoMSIA model correlates well with previous receptor-docking results, current SAR data of A_3AR agonists, and successful cases of the conversion of A_3AR agonists into antagonists by substitution of the characteristic 5′-*N*-methyluronamide moiety to introduce structural constraints or to reduce H-bonding ability. The excellent correlation with several experimental studies suggests that these 3D-QSAR models are valuable computational tools for both the rational design of novel A_3AR agonists and the prediction of agonist properties prior to experimentation.

The development of a quantitative SAR method for predicting pharmacological parameters of nucleosides acting at this therapeutically important AR subtype will aid in the ongoing design of new agonists. A novel aspect in this study is the application of the CoMFA/CoMSIA method to the relative efficacy of these nucleoside derivatives, in addition to its routine application to binding affinity. Thus, it is possible to predict not only binding affinity but also the maximal functional effect of a given compound at receptor-saturating concentrations.

EXPERIMENTAL SECTION

Molecular Modeling. All calculations were performed on a Silicon Graphics (Mountain View, CA) Octane2 workstation (600 MHz MIPS R14000 [IP30] processor). We used as the ligand starting conformation the crystal structure of adenosine monophosphate (PDB ID code: 1FTA)[29] with the 5′-phosphate group removed. This ligand has a conformation similar to the A_3AR-bound conformation, that is, Northern (*N*) and anti.[30] Adenosine analogues were then constructed with the Sketch Molecule of SYBYL7.1.[31] For all rotatable bonds, a random search was performed with a fixed (*N*)-anti form. The options of the random search were 3000 iterations, 3 kcal energy cutoffs, and chirality checking. In all cases, PM3 charges for electrostatic fields were applied to the lowest-energy conformer of each compound optimized by the MMFF94 with the use of distance-dependent dielectric constants and with the conjugate gradient method applied until the gradient reached 0.05 kcal mol^{-1} $Å^{-1}$.[32]

Data Sets. The K_i values for the training set (**1**−**91**) were converted to pK_i (−log K_i) values and used as dependent variables in the CoMFA and the CoMSIA studies. The relative efficacies (%) of full agonist Cl-IB-MECA values of the A_3AR were also used for the CoMSIA study, since the log values of the efficacies did not display reasonable statistical models because of a one-order difference. To further evaluate the predictability of the CoMFA and the CoMSIA models, a diverse collection of 25 compounds (**92**−**116**) was randomly selected from other data as an external test set, with some bias toward ensuring representation of the full range of biological data, and the binding affinities were predicted by the models (Figure I and Table III in the Supporting Information).

Alignments. Adenosine, an endogenous agonist, was selected as the template for aligning the compounds in the training set and with the test sets. All molecules from the database of the training set were suitably aligned into a similar orientation in Cartesian space with the "Align Database" module to achieve a rigid fitting of the common core of the molecules to a template. Specifically, all heteroatoms in adenosine, except the 4′-O atom, were chosen for the alignment, as a consequence of the inclusion of 4′-thioadenosine derivatives in the database.

Calculation of CoMFA and Hydrogen-Bond Fields. The standard CoMFA procedure as implemented in SYBYL7.1 was performed. A region file was automatically generated at least 4 Å beyond every molecule in all directions. Each ligand was placed in a 3D lattice with grid points sampled

at regular intervals by 1 or 2 Å in a defined region ($X = -22$ to -2, $Y = -16$ to $+16$, $Z = -8$ to $+8$). A C_{sp3} atom with a formal charge of $+1$ and a van der Waals radius of 1.52 Å served as the probe. The steric (van der Waals) and electrostatic (Coulombic) interactions were calculated at each of the grid points by summing the individual interaction energies between each atom of the ligand molecule and the probe atom. A distance-dependent dielectric function with a 1.0 dielectric constant was adopted for application of Coulomb's law. The computed field energies were truncated to 30 kcal/mol for the steric and electrostatic fields. HB fields as special indicator fields[33] were calculated. Lattice points were assigned an energy of 0, if they were not near HB acceptor or donor atoms or if H-bonding interactions were forbidden by steric congestion, defined by a steric cutoff of 50 kcal/mol. Lattice points in sterically allowed regions that were close to acceptor or donor atoms were assigned a nominal energy equal to the designated steric cutoff. In this technique, unlike in CoMSIA, donor and acceptor fields cannot be separated computationally, as the steric and electrostatic components of the Tripos standard fields can be.

Calculation of CoMSIA field. The CoMSIA analysis was performed with the QSAR module of SYBYL with the molecules embedded in a grid containing a regularly spaced common probe atom with a radius of 1 Å, a charge of $+1$, a hydrophobicity of $+1$, HB donating at $+1$, and HB accepting at $+1$. Five different similarity fields, including the steric, electrostatic, hydrophobic,[34] HB donor, and HB acceptor,[35] were calculated with Gaussian-type distance dependence between the probe and molecule atoms. The attenuation factor α for optimized q^2 values was set to 0.4.

Partial Least-Square Analysis. To measure the predictive power of the model through cross-validated r^2 values, partial least-square (PLS) analysis[36] was performed with the following options: "leave-one-out" cross-validation, a column scaling of CoMFA standard, and no column filtering. Sample-distance PLS[37] was prechecked to obtain more rapid results. The outlier points whose target values were badly predicted in the residual plot from the cross-validation analyses were omitted to get the predictable model with a sufficiently high q^2 value (>0.4). The final PLS analysis was then performed without cross-validation with an optimum number of components reported from the cross-validation results. To enhance or to attenuate the contribution of each of the grid points to subsequent analyses, a method of region focusing[38] was applied with StDev*Coefficient weights. The CoMSIA fields were scaled according to CoMFA standard deviation to give the same potential weights in the resulting QSAR.

Contour Details. All models were represented as color contour maps to enable the visualization of characteristic fields that significantly contribute to the A_3AR binding as well as to activation. The visualization of the CoMFA and CoMSIA maps was performed with the StDev*Coefficient mapping option contoured by contribution. Favored and disfavored levels fixed at 80% and 20%, respectively, were used for all fields. The steric contours are shown in green for regions tolerating greater steric bulk and yellow for regions requiring less bulky groups. The electrostatic maps are represented with blue contours indicating the regions where positive groups increased activity and red contours indicating regions where negative charge increased activity. In the CoMSIA result, the hydrophobic fields were colored in yellow for regions tolerating greater hydrophobicity and in white for regions tolerating greater hydrophilicity. The HB field contours showed regions that favor (in red) or disfavor (in magenta) HB acceptors and regions that favor (in cyan) or disfavor (in purple) HB donors.

ACKNOWLEDGMENT

This research was supported by the Intramural Research Program of the NIH, National Institute of Diabetes and Digestive and Kidney Diseases. We thank Dr. Andrei A. Ivanov, Krishnan K. Palaniappan, and Dr. Zhan-Guo Gao (NIDDK); Prof. Serge Van Calenbergh (University of Ghent, Belgium); and Prof. Lak Shin Jeong (EWHA Womens University, Seoul, Korea) for helpful discussions.

Supporting Information Available: Additional detailed results are provided. Tables I and III list the measured affinities of the adenosine derivatives in the training and test sets, respectively. Table II shows the comparison of experimental and predicted binding affinities and relative efficacies of adenosine derivatives at hA_3ARs in the training set. Figure I showing the structure of the adenosine derivatives in the training and test sets, Figure II showing a potent A_3AR agonist (Cl-IB-MECA) docked to the Connolly electrostatic potential surface of the hA_3AR, and Figure III showing the CoMSIA maps of the CoMSIA-2 and CoMSIA-EFF models are included. This material is available free of charge via the Internet at http://pubs.acs.org.

REFERENCES AND NOTES

(1) Fredholm, B. B.; IJzerman, A. P.; Jacobson, K. A.; Klotz, K.-N.; Linden, J. International Union of Pharmacology. XXV. Nomenclature and Classification of Adenosine Receptors. *Pharmacol. Rev.* **2001**, *53*, 527−552.

(2) Yan, L.; Burbiel, J. C.; Maass, A.; Müller, C. E. Adenosine Receptor Agonists: From Basic Medicinal Chemistry to Clinical Development. *Expert Opin. Emerging Drugs* **2003**, *8*, 537−576.

(3) Leesar, M. A.; Stoddard, M.; Ahmed, M.; Broadbent, J.; Bolli, R. Preconditioning of Human Myocardium with Adenosine during Coronary Angioplasty. *Circulation* **1997**, *95*, 2500−2507.

(4) Conti, J. B.; Belardinelli, L.; Curtis, A. B. Usefulness of Adenosine in Diagnosis of Tachyarrhythmias. *Am. J. Cardiol.* **1995**, *75*, 952−955.

(5) Madi, L.; Bar-Yehuda, S.; Barer, F.; Ardon, E.; Ochaion, A.; Fishman, P. J. A_3 Adenosine Receptor Activation in Melanoma Cells: Association between Receptor Fate and Tumor Growth Inhibition. *Biol. Chem.* **2003**, *278*, 42121−42130.

(6) Joshi, B. V.; Jacobson, K. A. Purine Derivatives as Ligands for A_3 Adenosine Receptors. *Curr. Top. Med. Chem. (Sharjah, United Arab Emirates)* **2005**, *5*, 1275−1295.

(7) Siddiqi, S. M.; Pearlstein, R. A.; Sanders, L. H.; Jacobson, K. A. Comparative Molecular Field Analysis of Selective A_3 Adenosine Agonists. *Bioorg. Med. Chem.* **1995**, *3*, 1331−1343.

(8) Rieger, J. M.; Brown, M. L.; Sullivan, G. W.; Linden, J.; Macdonald, T. L. Design, Synthesis, and Evaluation of Novel A_{2A} Adenosine Receptor Agonists. *J. Med. Chem.* **2001**, *44*, 531−539.

(9) Moro, S.; Bacilieri, M.; Ferrari, C.; Spalluto, G. Autocorrelation of Molecular Electrostatic Potential Surface Properties Combined with Partial Least Squares Analysis as Alternative Attractive Tool To Generate Ligand-Based 3D-QSARs. *Curr. Drug Discovery Technol.* **2005**, *2*, 13−21.

(10) Cramer, R. D., III; Patterson, D. E.; Bunce, J. D. Comparative Molecular Field Analysis (CoMFA). 1. Effect of Shape on Binding of Steroids to Carrier Proteins. *J. Am. Chem. Soc.* **1988**, *110*, 5959−5967.

(11) Cramer, R. D., III; DePriest, S. A.; Patterson, D. E.; Hecht, P. The Developing Practice of Comparative Molecular Field Analysis. In *3D QSAR in Drug Design: Theory, Methods and Applications*; Kubinyi, H., Ed.; ESCOM: Leiden, Netherlands, 1993; pp 443−485.

(12) Li, A.-H.; Moro, S.; Forsyth, N.; Melman, N.; Ji, X.-d.; Jacobson, K. A. Synthesis, CoMFA Analysis, and Receptor Docking of 3,5-Diacyl-

2,4-dialkylpyridine Derivatives as Selective A_3 Adenosine Receptor Antagonists. *J. Med. Chem.* **1999**, *42*, 706−721.
(13) Klebe, G.; Abraham, U.; Mietzner, T. Molecular Similarity Indices in a Comparative Analysis (CoMSIA) of Drug Molecules to Correlate and Predict Their Biological Activity. *J. Med. Chem.* **1994**, *37*, 4130−4146.
(14) Tchilibon, S.; Kim, S. K.; Gao, Z. G.; Harris, B. A.; Blaustein, J. B.; Gross, A. S.; Duong, H. T.; Melman, N.; Jacobson, K. A. Exploring Distal Regions of the A_3 Adenosine Receptor Binding Site: Sterically Constrained N^6-(2-phenylethyl) Adenosine Derivatives as Potent Ligands. *Bioorg. Med. Chem.* **2004**, *12*, 2021−2034.
(15) Ohno, M.; Gao, Z. G.; Van Rompaey, P.; Tchilibon, S.; Kim, S. K.; Harris, B. A.; Gross, A. S.; Duong, H. T.; Van Calenbergh, S.; Jacobson, K. A. Modulation of Adenosine Receptor Affinity and Intrinsic Efficacy in Adenine Nucleosides Substituted at the 2-Position. *Bioorg. Med. Chem.* **2004**, *12*, 2995−3007.
(16) Gao, Z. G.; Mamedova, L.; Chen, P.; Jacobson, K. A. 2-Substituted Adenosine Derivatives: Affinity and Efficacy at Four Subtypes of Human Adenosine Receptors. *Biochem. Pharmacol.* **2004**, *68*, 1985−1993.
(17) Jeong, L. S.; Lee, H. W.; Kim, H. O.; Jung, J. Y.; Gao, Z. G.; Duong, H. T.; Rao, S.; Jacobson, K. A.; Shin, D. H.; Lee, J. A.; Gunaga, P.; Lee, S. K.; Jin, D. Z.; Chun, M. W. Design, Synthesis, and Biological Activity of N^6-Substituted-4′-thioadenosines at the Human A_3 Adenosine Receptor. *Bioorg. Med. Chem.* **2006**, *14*, 4718−4730.
(18) Jeong, L. S.; Lee, H. W.; Jacobson, K. A.; Kim, H. O.; Shin, D. H.; Lee, J. A.; Gao, Z. G.; Lu, C.; Duong, H. T.; Gunaga, P.; Lee, S. K.; Jin, D. Z.; Chun, M. W.; Moon, H. R. Structure−Activity Relationships of 2-Chloro-N^6-substituted-4′-thioadenosine-5′-uronamides as Highly Potent and Selective Agonists at the Human A_3 Adenosine Receptor. *J. Med. Chem.* **2006**, *49*, 273−281.
(19) Gao, Z. G.; Blaustein, J.; Gross, A. S.; Melman, N.; Jacobson, K. A. N^6-Substituted Adenosine Derivatives: Selectivity, Efficacy, and Species Differences at A_3 Adenosine Receptors. *Biochem. Pharmacol.* **2003**, *65*, 1675−1684.
(20) Van Rompaey, P.; Jacobson, K. A.; Gross, A. S.; Gao, Z. G.; Van Calenbergh, S. Exploring Human Adenosine A_3 Receptor Complementarity and Activity for Adenosine Analogues Modified in the Ribose and Purine Moiety. *Bioorg. Med. Chem.* **2005**, *13*, 973−983.
(21) Cosyn, L.; Palaniappan, K. K.; Kim, S. K.; Duong, H. T.; Gao, Z.-G.; Jacobson, K. A.; Van Calenbergh, S. 2-Triazole-substituted Adenosines: A New Class of Selective A_3 Adenosine Receptor Agonists, Partial Agonists, and Antagonists. *J. Med. Chem.* **2006**, *49*, 7373−7383.
(22) Peng, Y.; Keenan, S. M.; Zhang, Q.; Kholodovych, V.; Welsh, W. J. 3D-QSAR Comparative Molecular Field Analysis on Opioid Receptor Antagonists: Pooling Data from Different Studies. *J. Med. Chem.* **2005**, *48*, 1620−1629.
(23) Kim, S-K.; Gao, Z. G.; Jeong, L. S.; Jacobson, K. A. Docking Studies of Agonists and Antagonists Suggest an Activation Pathway of the A_3 Adenosine Receptor. *J. Mol. Graphics Model.* **2006**, *25*, 562−577.
(24) Gao, Z. G.; Kim, S. K.; Biadatti, T.; Chen, W.; Lee, K.; Barak, D.; Kim, S. G.; Johnson, C. R.; Jacobson, K. A. Structural Determinants of A_3 Adenosine Receptor Activation: Nucleoside Ligands at the Agonist/Antagonist Boundary. *J. Med. Chem.* **2002**, *45*, 4471−4484.
(25) Gao, Z. G.; Kim, S. K.; Gross, A. S.; Chen, A.; Blaustein, J. B.; Jacobson, K. A. Identification of Essential Residues Involved in the Allosteric Modulation of the Human A_3 Adenosine Receptor. *Mol. Pharmacol.* **2003**, *63*, 1021−1031.
(26) Jacobson, K. A.; Gao, Z. G.; Chen, A.; Barak, D.; Kim, S-A.; Lee, K.; Link, A.; Van Rompaey, P. V.; Van Calenbergh, S.; Liang, B. T. Neoceptor Concept Based on Molecular Complementarity in GPCRs: A Mutant Adenosine A_3 Receptor with Selectivity Enhanced Affinity for Amine-Modified Nucleosides. *J. Med. Chem.* **2001**, *44*, 4125−4136.
(27) van Tilburg, E. W.; von Frijtag Drabbe Künzel, J.; de Groote, M.; Vollinga, R. C.; Lorenzen, A.; IJzerman, A. P. N^6, 5′-Disubstituted Adenosine Derivatives as Partial Agonists for the Human Adenosine A_3 Receptor. *J. Med. Chem.* **1999**, *42*, 1393−1400.
(28) Gao, Z. G.; Joshi, B. V.; Klutz, A.; Kim, S. K.; Lee, H. W.; Kim, H. O.; Jeong, L. S.; Jacobson, K. A. Conversion of A_3 Adenosine Receptor Agonists into Selective Antagonists by Modification of the 5′-Ribofuran-uronamide Moiety. *Bioorg. Med. Chem. Lett.* **2006**, *16*, 596−601.
(29) Gidh-Jain, M.; Zhang, Y.; van Poeljen, P. D.; Liang, J-Y.; Huang, S.; Kim, J.; Elliott, J. T.; Erion, M. D.; Pilkis, S. J.; El-Maghrabi, M. R.; Lipscomb, W. N. The Allosteric Site of Human Liver Fructose-1,6-bisphosphatase. Analysis of Six AMP Site Mutants Based on the Crystal Structure. *J. Biol. Chem.* **1994**, *269*, 27732−27738.
(30) Jacobson, K. A.; Ji, X.-d.; Li, A. H.; Melman, N.; Siddiqui, M. A.; Shin, K. J.; Marquez, V. E.; Ravi, R. G. Methanocarba Analogues of Purine Nucleosides as Potent and Selective Adenosine Receptor Agonists. *J. Med. Chem.* **2000**, *43*, 2196−2203.
(31) *SYBYL*, version 7.1; Tripos Inc.: St. Louis, MO, 2005.
(32) Halgren T. A. Characterization of MMFF94, MMFF94s, and Other Widely Available Force Fields for Conformational Energies and for Intermolecular-Interaction Energies and Geometries. *J. Comput. Chem.* **1999**, *20*, 730−748.
(33) Bohacek, R. S.; McMartin, C. Definition and Display of Steric, Hydrophobic, and Hydrogen-Bonding Properties of Ligand Binding Sites in Proteins using Lee and Richards Accessible Surface: Validation of a High-Resolution Graphical Tool for Drug Design. *J. Med. Chem.* **1992**, *35*, 1671−1684.
(34) Viswanadhan, V. N.; Ghose, A. K.; Revenkar, G. R.; Robins, R. K. Physicochemical Parameters for Three-Dimensional Structure-Directed Quantitative Structure−Activity Relationships. 4. Additional Parameters for Hydrophobic and Dispersive Interactions and Their Application for an Automated Superposition of Certain Naturally Occurring Nucleoside Antibiotics. *J. Chem. Inf. Comput. Sci.* **1989**, *29*, 163−172.
(35) Klebe, G.; Abraham, U. Comparative Molecular Similarity Index Analysis (CoMSIA) to Study Hydrogen Bonding Properties and to Score Combinatorial Libraries. *J. Comput.-Aided Mol. Des.* **1999**, *13*, 1−10.
(36) Stahle, L.; Wold, S. Multivariate Data Analysis and Experimental Design in Biomedical Research. *Prog. Med. Chem.* **1988**, *25*, 291−338.
(37) Bush, B. L.; Nachbar, R. B. Sample-Distance Partial Least Squares: PLS Optimized for Many Variables, with Application to CoMFA. *J. Comput.-Aided Mol. Des.* **1993**, *7*, 587−619.
(38) Forina, M.; Casolino, C.; Pizarro Millan, C. Iterative Predictor Weighting (IPW) PLS. Part 1. A Technique for the Elimination of Useless Predictors in Regression Problems. *J. Chemom.* **1999**, *13*, 165−184.
(39) Fredholm, B. B.; Irenius, E.; Kull, B.; Schulte, G. Comparison of the Potency of Adenosine as an Agonist at Human Adenosine Receptors Expressed in Chinese Hamster Ovary Cells. *Biochem. Pharmacol.* **2001**, *61*, 443−448.

CI600501Z